2D Fokker–Planck models of rotating clusters

J. Fiestas,[1,2]⋆ R. Spurzem,[1,2]⋆ and E. Kim[3]⋆

[1]*Astronomisches Rechen-Institut, Zentrum für Astronomie, Universität Heidelberg, Mönchhofstraße 12-14, D-69120 Heidelberg, Germany*
[2]*The Rhine Stellar-Dynamical Network*
[3]*Harvard–Smithsonian Center for Astrophysics, 60 Garden Street, Cambridge, MA 02138, USA*

ABSTRACT

Globular clusters rotate significantly, and with the increasing amount of detailed morphological and kinematical data obtained in recent years on galactic globular clusters many interesting features show up. We show how our theoretical evolutionary models of rotating clusters can be used to obtain fits, which at least properly model the overall rotation and its implied kinematics in full 2D detail (dispersions, rotation velocities). Our simplified equal mass axisymmetric rotating model provides detailed two-dimensional kinematical and morphological data for star clusters. The degree of rotation is not dominant in energy, but also non-negligible for the phase-space distribution function, shape and kinematics of clusters. Therefore, the models are well applicable for galactic globular clusters. Since previously published papers on that matter by us made it difficult to do detailed comparisons with observations, we provide a much more comprehensive and easy-to-use set of data here, which uses as entries dynamical age and flattening of observed cluster and then offers a limited range of applicable models in full detail. The method, data structure and some exemplary comparison with observations are presented. Future work will improve modelling and data base to take a central black hole, a mass spectrum and stellar evolution into account.

Key words: gravitation – stellar dynamics – methods: numerical – globular clusters: general.

1 INTRODUCTION

Many globular clusters do show some amount of rotation, even the old ones of our own Galaxy (Meylan & Mayor 1986; Lupton, Gunn & Griffin 1987 and some 10 others, K. Gebhardt, personal communication). The more accurate and star-by-star observations become available, the more important it is to properly model the effects of rotation together with evolution of globular star clusters, since typically the amount of rotational energy in clusters is not dominant, but also not negligible. It is long known that indeed flattenings of galactic globular clusters correlate with their rotation, suggesting that rotation still is important for the shape (White & Shawl 1987). Proper motions of stars in ωCen have been measured to get a real 3D profile of stellar motions including rotation, and in fantastic improvements of observations using the *Hubble Space Telescope* (*HST*) it became even possible to measure rotation of 47Tuc in the plane of the sky (Anderson & King 2003). While without rotation the wealth of observational data such as luminosity functions and derived mass functions, colour–magnitude diagrams and population and kinematical analysis, obtained by e.g. the *HST*, for extragalactic as well as Milky Way clusters (cf. e.g. Barmby, Holland & Huchra 2002; Piotto et al. 2002; Pulone et al. 2003; Rich et al. 2005; Zhao

& Bailyn 2005; Beccari et al. 2006, to mention only the few most recently appeared papers), is balanced by a decent amount of detailed modelling (see below), theorists and observers alike seem to be appallingly puzzled by rotation in clusters, and are disappointed that (multimass) King model fitting does not work very well (see e.g. Piotto et al. 1999, and for a specific example McLaughlin et al. 2003, therein).

One notable exception being the early three integral models by Lupton et al. (1987) nobody seemed to care about rotation in globular cluster modelling since then for a long time. There was a thesis by Jeremy Goodman (1983), whose part on rotation of clusters remained unpublished, but who was the pioneer for the main idea to use a two-dimensional approximation using the distribution function as function of energy E and z-component of angular momentum J_z, and neglect the possible dependencies on a third integral I_3 for the time being. Unfortunately, the solution of the 2D orbit-averaged Fokker–Planck (henceforth FP) equation, including the self-consistent numerical determination of diffusion coefficients, is an extremely complex numerical problem, involving two levels of numerical integrations in a second-order integro-differential equations, in other words we need 4D nested discretization in E, J_z, ϖ and z where the latter are the spatial coordinates. It turned out that the problem was too challenging in the mid-eighties for the then available computers. With the help of Goodman, who kindly made his PhD thesis available at an early stage, Einsel & Spurzem (1999, Paper I) could rewrite from scratch a new FP code and publish a

⋆E-mail: fiestas@ari.uni-heidelberg.de (JF); spurzem@ari.uni-heidelberg.de (RS); ekim@head.cfa.harvard.edu (EK)

sequence of rotating cluster models (pre-collapse, equal masses). These studies have been recently improved in a comprehensive effort on the FP side (Kim et al. 2002, hereafter Paper II; Kim, Lee & Spurzem 2004, hereafter Paper III), and also promising results exist which show that the neglect of the third integral does not harm too much (if flattening is not extreme), since there is fair agreement with direct *N*-body models (see some examples in Paper II and Boily & Spurzem 2000). In a new approach (Ardi, Spurzem & Mineshige 2005), we are working to back up the amount of good *N*-body data for rotating clusters by a large number of small *N* averaged models and a few large models, as was done for the non-rotating case by Giersz & Heggie (1994, 1996) and Giersz & Spurzem (1994). It is clear that while all work known to the authors at this moment concentrates on self-gravitating star clusters, the improvement of our knowledge and methods in the field of rotating dense stellar systems is extremely important for galactic nuclei, too, where a central star-accreting black hole comes into the game (some stationary modelling exists, such as Quinlan & Shapiro 1990; Murphy, Cohn & Durisen 1991; Freitag & Benz 2002). Also, claims have been made that some globular clusters in the halo of our Galaxy and around M31 contain massive black holes (Gerssen et al. 2002), and these results have been challenged by Baumgardt et al. (2003). However, the latest paper could only provide a very limited number of case studies, due to the enormous computing time needed even on the GRAPE computers. Therefore, it is very urgent to develop reliable approximate models of rotating star clusters with black hole, which is subject of current work.

Dynamical modelling of globular clusters and other collisional stellar systems (like galactic nuclei, rich open clusters and rich galaxy clusters) still poses a considerable challenge for both theory and computational requirements (in hardware and software). On the theoretical side, the validity of certain assumptions used in statistical modelling based on the FP and other approximations is still poorly known. Stochastic noise in a discrete *N*-body system and the impossibility to directly model realistic particle numbers with the presently available hardware, are a considerable challenge for the computational side.

A large amount of individual pair wise forces between particles needs to be explicitly calculated to properly follow relaxation effects based on the cumulative effects of small angle gravitative encounters. Therefore, modelling of globular star clusters over their entire lifetime requires a star-by-star simulation approach, which is highly accurate in following stellar two- and many-body encounters. Distant two-body encounters, the backbone of quasi-stationary relaxation processes, have to be treated properly by the integration method directly, while close encounters, in order to avoid truncation errors and downgrading of the overall performance, are treated in relative and specially regularized coordinates (Kustaanheimo & Stiefel 1965; Mikkola & Aarseth 1998), their centres of masses being used in the main integrator. The factual world standard of such codes has been set by Aarseth and his codes NBODY*n* codes ($0 \leqslant n \leqslant 7$; see Aarseth 1999a,b, 2003). Another integrator KIRA aimed at high-precision has been used (McMillan & Hut 1996; Portegies Zwart et al. 1998; Takahashi & Portegies Zwart 2000). It uses a hierarchical binary tree to handle compact subsystems instead of regularization.

Unfortunately, the direct simulation of most dense stellar systems with star-by-star modelling is not yet possible, although recent years have seen a significant progress in both hardware and software (Makino & Taiji 1998; Aarseth 1999a,b; Spurzem 1999; Makino 2005). Despite such progress in hardware and software even the largest useful direct *N*-body models for both globular cluster and

galactic nuclei evolution have still not yet reached the realistic particle numbers ($N \sim 5 \times 10^5$ for globular clusters, $N \sim 10^6$–10^9 for galactic nuclei). However, recent work by Baumgardt, Hut & Heggie (2002) and Baumgardt & Makino (2003) has pushed the limits of present direct modelling for the first time to some 10^5 using either NBODY6++ on parallel computers or NBODY4 on GRAPE-6 special purpose hardware. There is a notable exception of a direct one-million body problem with a central binary black hole tackled by Hemsendorf, Dorband & Merritt (2003). Their code, however, being very innovative for the large *N* force calculation, still lacks the fine ingredients of treating close encounters between stars and black hole particles from the standard *N*-body codes.

Bridging the gap between direct models and the most interesting particle numbers in real systems is far from straightforward, neither by scaling (Baumgardt 2001), nor by theory. There are two main classes of theory: (i) FP models, which are based on the direct numerical solution of the orbit-averaged FP equation (Cohn 1979; Murphy et al. 1991) and (ii) isotropic (Lynden-Bell & Eggleton 1980; Heggie 1984) and anisotropic gaseous models (Giersz & Spurzem 1994; Spurzem 1996), which can be thought of as a set of moment equations of the FP equation.

On the side of the direct FP models there have been two major recent developments. Takahashi (1995, 1996, 1997) has published new FP models for spherically symmetric star clusters, based on the numerical solution of the orbit-averaged 2D FP equation (solving the FP equation for the distribution $f = f(E, J^2)$ as a function of energy and angular momentum, on an (E, J^2) mesh). Drukier et al. (1999) have published results from another 2D FP code based on the original Cohn (1979) code. In such 2D FP models anisotropy, i.e. the possible difference between radial and tangential velocity dispersions in spherical clusters, is taken into account.

Secondly, another 2D FP model has been worked out recently for the case of axisymmetric rotating star clusters (Paper I; Paper II). Here, the distribution function is assumed to be a function of energy E and the z-component of angular momentum J_z only; a possible dependence of the distribution function on a third integral is neglected. As in the spherically symmetric case, the neglection of an integral of motion is equivalent to the assumption of isotropy, here between the velocity dispersions in the meridional plane (*r* and *z* directions); anisotropy between velocity dispersion in the meridional plane and that in the equatorial plane (ϕ direction), however, is included. We realize that the evolutionary models provided by us for rotating globular clusters are difficult to use for direct comparisons with observations, because they are not easily analytically describable. However, they are the only ones which fully cope with *all* observational data available nowadays (full 3D velocity data, including velocity dispersions in ϖ and ϕ directions, rotational velocity, density, all as full 2D functions of ϖ and *z*). No other evolutionary model exists so far which is able to provide this information. With the advent of our new post-collapse and multimass models (Paper II; Paper III), and the inclusion of stellar evolution and binaries (work in progress) we will be able to deliver even more interesting results. Already the existing *N*-body study (Ardi et al. 2005) shows that rotation not only accelerates the collisional evolution but also leads to an increasing binary activity in the system.

Here we present a detailed and comprehensive set of our model data, covering a fair range of rotation rates and initial concentrations of galactic globular clusters, which is aimed to enable observers to use them for comparison with their data. The basic idea is to start up with a dynamical cluster age and a present day observed flattening, and then being able to pick a number of models from our evolutionary model data base which allow a prediction (within certain

ambiguity) of how this clusters started up initially. In this paper, we present the basic procedure of modelling and how we create the data, and give a few exemplary data to show the capabilities of our data base which is to be found in the web (http://www.ari.uni-heidelberg.de/clusterdata).

Sections 2 and 3 summarize briefly the numerical and physical procedure used for our evolving rotating cluster models, and the choice of initial conditions. Section 4 describes the comprehensive set of data we provide for every of our models using one example set, and Section 5 shows how observational data can be used to obtain the proper entry points in our data for a more detailed theory–observation comparison.

2 THEORETICAL MODEL

The stellar system is assumed to be axisymmetric [cylindrical coordinates (ϖ, z, φ) were used] and in dynamical equilibrium. Therefore, the distribution function $f(\varpi, z, \varphi)$ is almost constant on the dynamical time-scale. The only classical isolating integrals of a general axisymmetric potential ϕ are the energy per unit mass

$$E = \frac{1}{2}v^2 + \phi(\varpi, z) \tag{1}$$

and the component of angular momentum along the z-axis per unit mass

$$J_z = \varpi\, v_\varphi \tag{2}$$

(E and ϕ are negative for bound particles).

The Boltzmann equation written in terms of E and J_z has to be evaluated in the code

$$\frac{\partial f}{\partial t} + \frac{\partial \phi}{\partial t}\frac{\partial f}{\partial E} = \left(\frac{\partial f}{\partial t}\right)_{\text{coll}}, \tag{3}$$

where $f(E, J_z, I_3)$ is the distribution function in axial symmetry. Here, I_3 represents a third integral, which is neglected in the model (see Paper I, for a discussion of possible errors).

Small angle scattering ($\Delta v/v \ll 1$) is a condition for the expansion of the FP approximation. Diffusion coefficients of third and higher order are neglected. Thus, the collision term on the right-hand side of equation (3) is given by

$$\left(\frac{\partial f}{\partial t}\right)_{\text{coll}} = \frac{1}{V}\left[-\frac{\partial}{\partial E}(\langle\Delta E\rangle fV) - \frac{\partial}{\partial J_z}(\langle\Delta J_z\rangle fV)\right.$$
$$+ \frac{1}{2}\frac{\partial^2}{\partial E^2}(\langle\Delta E^2\rangle fV) + \frac{\partial^2}{\partial E\partial J_z}(\langle\Delta E\Delta J_z\rangle fV)$$
$$\left. + \frac{1}{2}\frac{\partial^2}{\partial J_z^2}(\langle\Delta J_z^2\rangle fV)\right], \tag{4}$$

where V is the volume element given by $2\pi/\varpi$.

Due to the relation $t_r \gg t_{\text{dyn}}$ (for globular clusters is $t_r \sim 10^9$ yr $\sim 10^3 t_{\text{dyn}}$), the orbit will spread only on a relaxation time-scale (because of encounters and assuming a conserved third integral). Therefore, an orbit average of the FP equation is taken over an area in the meridional plane that intersects the hypersurface in phase space with the same E and J_z.

Furthermore, the physical variables E and J_z are transformed to the suitable dimensionless quantities X and Y. The choice of $X(E) \equiv \ln[E/(2\phi_c - E_0 - E)]$, where E_0 is the energy of a circular orbit at the core radius of the cluster, guarantees a good resolution in energy space both for small energies and for the energy belonging to the central particles. $Y(J_z, E) \equiv J_z/J_z^{\text{max}}$ is a dimensionless z-component of angular momentum ($0 < |Y| < 1$). A rectangular mesh

is generated on which the FP equation is discretized. The models presented use a number grid size in (X, Y) of (100×61). The relative error in energy conservation using this configuration is less than 0.7 per cent.

The orbit-averaged flux coefficients are derived from the local diffusion coefficients, which are found for the axial symmetric geometry via the prescriptions of Rosenbluth (1957) involving covariant derivatives instead of the procedure employed by Goodman (1983) using a non-covariant form. The derivation of the diffusion coefficients makes it necessary to specify a background distribution function by which test stars are scattered. Using the foreground distribution for the background self-consistently would require computational time proportional to $N_\varpi \times N_z \times N_E^2 \times N_{J_z}^2$, where the N_i are grid sizes in coordinate and velocity space, which would reduce the grids employed to inaccurate descriptions of the current problem; thus, as in all previous applications concerning two-dimensional FP methods for stellar systems, we set up an appropriate form of the background distribution. Herein we follow Goodman (1983), giving a rotating Maxwellian velocity distribution to the background, thereby reducing the computational efforts necessary.

The following steps are taken in the code.[1]

(i) Construction of initial rotating King models [initial potential $\phi(\varpi, z)$ and density $n(\varpi, z)$ pairs are computed]

(ii) The evolution due to stellar collisions is calculated in the FP step using the method described by Henyey et al. (1959), while $\phi(\varpi, z)$ is constant

(iii) Recalculation of f due to slow changes in the potential (Vlasov step).

3 INITIAL CONDITIONS

The initial models are rotating King models of the form

$$f_{\text{rk}}(E, J_z) = \text{const} \times [\exp(-\beta E) - 1] \exp(-\beta\Omega_0 J_z). \tag{5}$$

Initial parameters are
$\omega_0 = \sqrt{9/(4\pi G n_c)}\,\Omega_0$ is the dimensionless angular velocity,
$W_0 = -\beta(\phi - \phi_t)$ is the dimensionless central potential,
where $\beta = 1/\sigma_c^2$, σ_c is the central one-dimensional velocity dispersion and n_c is the central density.

Time units are defined as follows.
Dynamical time t_0:

$$t_0 = \sqrt{\frac{r_{c_i}^3}{GM_i}}\frac{(GM_i)^2}{4\pi\Gamma}\frac{1}{N}, \qquad \text{(Cohn 1979)}. \tag{6}$$

Where, $M_i(\equiv 1)$ is the initial total cluster mass; $r_{c_i}(=1)$, the initial core radius; N is the total number of particles and $\Gamma = 4\pi G^2 (M_i/N)^2 \ln\Lambda$ ($\ln\Lambda$ is the Coulomb logarithm). The gravitational constant G is set to 1.
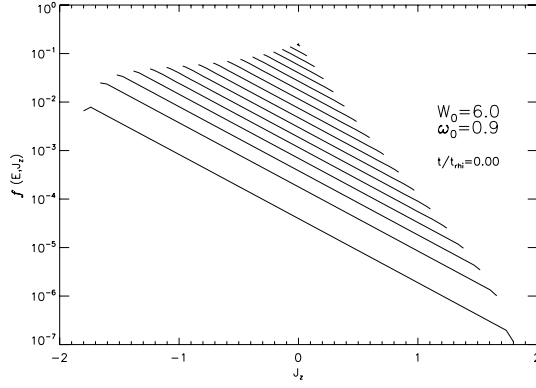
The initial half-mass relaxation time is defined as (Spitzer & Hart 1971)

$$t_{\text{rh}_i} = 0.138N\sqrt{\frac{r_{h_i}^3}{GM_i}}\frac{1}{\ln\Lambda}, \tag{7}$$

where r_{h_i} is the initial half-mass radius. Following the condition $t_0 \equiv 1$, evolution of t_{rh} can be calculated as

$$t_{\text{rh}} = 2.208\pi^2\sqrt{Mr_h^3}, \tag{8}$$

[1] This method, first developed for spherical systems in 1D by Cohn (1979), was originally used by Goodman (1983) in his unpublished PhD thesis.

Figure 1. Distribution function $f(E, J_z)$ against J_z for the model ($W_0 = 6$, $\omega_0 = 0.9$) at $t = 0 \, t_{\mathrm{rh_i}}$.

where M and r_{h} are the current total mass and half-mass radius. The cluster radius is given by

$$r_{\mathrm{c}} \equiv \sqrt{\frac{9\sigma_{\mathrm{c}}^2}{4\pi G n_{\mathrm{c}}}}. \tag{9}$$

The dynamical ellipticity e_{dyn} of the cluster is calculated following Goodman (1983), as

$$\frac{2T_{\mathrm{rot}} + 3T_{\sigma_\phi} - T_\sigma}{T_\sigma - T_{\sigma_\phi}} = \frac{(1 - 2s^2)\arccos s - 3s\sqrt{1 - s^2}}{s\sqrt{1 - s^2} - s^2 \arccos s}, \tag{10}$$

where $s \equiv b/a = 1 - e_{\mathrm{dyn}}$, T_{rot} is the rotational energy, T_{σ_ϕ} is the energy contained in the azimuthal component of the velocity dispersion and T_σ is the energy of all components of the velocity dispersion.

The cluster orbits its parent galaxy in a spherical potential, at a constant distance (circular orbit and constant mean density within the tidal radius). Stars are removed instantaneously beyond r_{t} using an energy criteria, i.e. if they have an energy larger than $E_{\mathrm{t}}(r_{\mathrm{t}})$, evaluated at every Poisson step.

4 NUMERICAL RESULTS

We describe in the Appendix a set of numerical simulations classified by ellipticity e_{dyn} and age of the system t/t_{rh}. The data base contains following evolutionary parameters.

(i) 2D parameters.
    (a) distribution function $f(E, J_z)$,
    (b) density $n(\varpi, z)$,
    (c) one-dimensional velocity dispersions $\sigma_\phi(\varpi, z)$ (azimuthal) and $\sigma_r (= \sigma_z)$ (in meridional plane),
    (d) rotational velocity $v_{\mathrm{rot}}(\varpi, z)$ and angular velocity $\Omega(\varpi, z)$,
    (e) potential $\phi(\varpi, z)$ and anisotropy $A(\varpi, z)$.
(ii) Global structure parameters like concentration $c = \log(r_{\mathrm{t}}/r_{\mathrm{c}})$, $(r_{\mathrm{c}}/r_{\mathrm{h}})$, escape energy and total mass.[2]

The following is a sample of the data base.

In Fig. 1, we show the dependence of the distribution function on the angular momentum for the initial model $W_0 = 6$, $\omega_0 = 0.9$ (moderate concentration, high initial rotation) at initial time. $f(E, J_z)$ for different J_z and the same energy E is represented by lines. Lines of higher energy (in the core) are narrower (due to the lower values

---

[2] See the Appendix for description of data and access to data base.
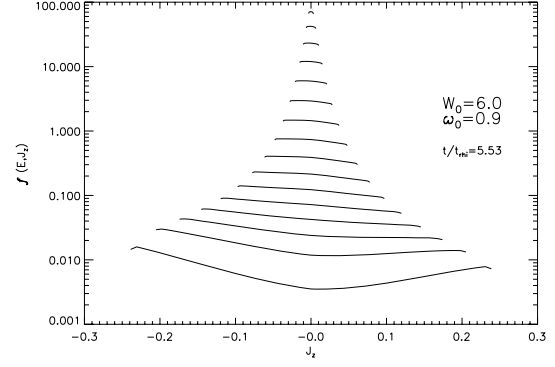
Figure 2. Distribution function $f(E, J_z)$ against J_z for the model ($W_0 = 6$, $\omega_0 = 0.9$) at $t = 5.53 \, t_{\mathrm{rh_i}}$.

of maximal angular momentum). The slope of each curve represents the exponent in the King distribution (equation 5). For comparison, we show $f(E, J_z)$ for the same model, at a later time (Fig. 2). We see that the slopes of the curves (rotation) change depending on the energy. They are not King models any more, and the initial relation between f and Ω_0 is not conserved. Changes in anisotropy (see definition in the Appendix) can be also observed in Fig. 2, where orbits lower energy (bottom curves) are slightly depleted around $J_z = 0$ (more circular orbits, negative anisotropy). At the same time, one can observe positive anisotropy built by orbits of higher energy (top curves), where f is enhanced around $J_z = 0$ (more radial orbits).

Although the main source of numerical error was detected in the recalculation of f due to small changes in the potential (Vlasov step), where a second-order interpolation of f is carried on; the relative error in f, accumulated over all grid cells per time-step, is not larger than 10^{-5}, which makes the numerical integration stable. The sharp bends at both ends of the lines of constant energy in Figs 1 and 2 visualize these errors. Moreover, rotating and non-rotating models show nearly the same energy conservation accumulated errors [~ 0.7 per cent for a grid $(N_E, N_{J_z}) = (100,61)$].

Fig. 3 shows the evolution of the central density for 11 models with different rotation ω_0 and potential W_0 parameters. The models with smaller parameter ω_0 reach collapse in longer times. Stronger rotating models show smaller collapse times. For comparison, we include here the models $W_0 = 6, 7, 8$. See Paper I, Paper II and
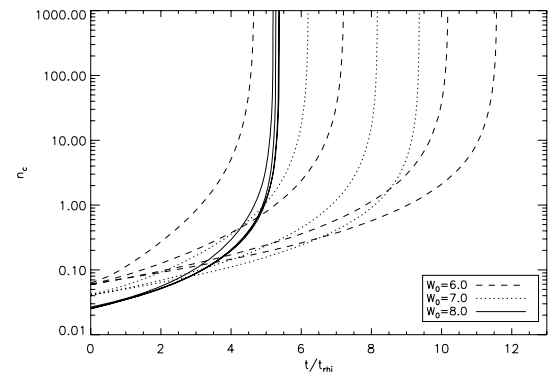
Figure 3. Central density n_{c} against time $t/t_{\mathrm{rh_i}}$ for models with $W_0 = 6$ (dashed lines), $W_0 = 7$ (dotted lines) and $W_0 = 8$ (solid lines). The rotation parameter $\omega_0 = 0.0, 0.3, 0.5, 0.7$ (for $W_0 = 6$), $\omega_0 = 0.0, 0.3, 0.5$ (for $W_0 = 7$) and $\omega_0 = 0.1, 0.15, 0.2, 0.3$ (for $W_0 = 8$) increases from right to left at the upper time axis.
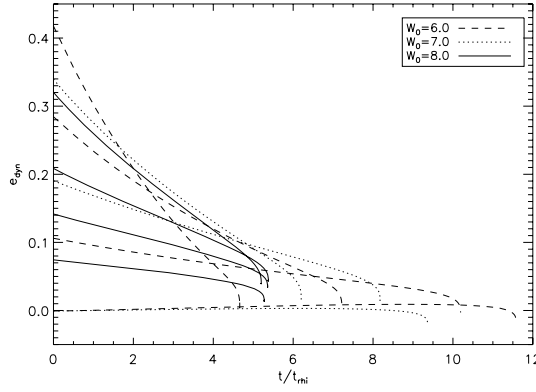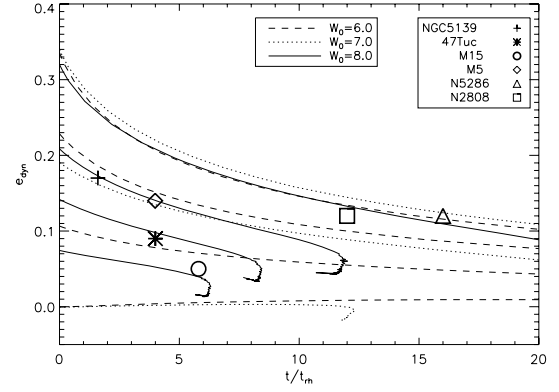
Figure 4. Dynamical ellipticity $e_{\rm dyn}$ against time $t/t_{\rm rh_i}$ for models with $W_0 = 6$ (dashed lines), $W_0 = 7$ (dotted lines) and $W_0 = 8$ (solid lines). The rotation parameter $\omega_0 = 0.0, 0.3, 0.5, 0.7$ (for $W_0 = 6$), $\omega_0 = 0.0, 0.3, 0.5$ (for $W_0 = 7$) and $\omega_0 = 0.1, 0.15, 0.2, 0.3$ (for $W_0 = 8$) increases from bottom to top at the $e_{\rm dyn}$ axis.

Figure 5. Time evolution (in units of current $t_{\rm rh}$) of dynamical ellipticity. The rotation parameter $\omega_0 = 0.0, 0.3, 0.5, 0.7$ (for $W_0 = 6$), $\omega_0 = 0.0, 0.3, 0.5$ (for $W_0 = 7$) and $\omega_0 = 0.1, 0.15, 0.2, 0.3$ (for $W_0 = 8$) increases from bottom to top at the $e_{\rm dyn}$ axis.

Paper III for further discussion on collapse times. Similarly, in Fig. 4 we show the evolution of dynamical ellipticity for the same models, as presented in Einsel & Spurzem (1999, Paper I) (their fig. 7). As observed, ellipticity decreases steeply for the initially most strongly rotating models and the final states of all models lack significant flattening. Note that the curves can cross each other, due to less effective angular momentum transport beyond the tidal boundary, in the more moderately rotating models. In Figs 3 and 4, evolution is given in units of initial $t_{\rm rh}$.

5 OBSERVATIONAL DATA COMPARISON

Observations show that flattening is a common feature of globular clusters. Geyer, Nelles & Hopp (1983) observed the radial variation of the ellipticity of 20 Galactic globular clusters and four clusters in the Large Magellanic Cloud. They found a general trend in ellipticity in a sense that in the inner and outer cluster regions they appear more circular and the ellipticity reaches a maximum at $\sim 1/3$ of the observable cluster extension. White & Shawl (1987) have measured the projected axial ratio (b/a) of 100 globular clusters in the Milky Way, where a and b denoted the semimajor and semiminor radii, respectively. They obtained that the mean axial ratio $\langle a/b \rangle = 0.93 \pm 0.01$ corresponding to $\langle \epsilon \rangle = 0.07 \pm 0.01$, where $\epsilon = 1 - b/a$. They argued that the flattened shape of the clusters can be caused by either anisotropy in velocity dispersion or rotation.

Meylan & Mayor (1986) and Merritt, Meylan & Mayor (1997) studied globular clusters in our Galaxy to reveal without ambiguity the global rotation in clusters such as ωCen and 47Tuc. *HST* observations of globular clusters provide data on the velocity field of globular clusters to high accuracy (Van Leeuwen et al. 2000; Anderson & King 2003). We look forward to have direct integration models to compare with these data.

Table 1 gives observational data for six globular clusters with ellipticities larger than zero and 2 with $e = 0$. The data were taken from the Harris catalogue of Milky Way globular clusters (Harris 1996, 2003 February revision). The columns of the table are as follows.
Column 1: cluster identification number.
Column 2: $r_{\rm c}$, current core radius in arcmin.
Column 3: $r_{\rm h}$, current half-mass radius in arcmin.
Column 4: $r_{\rm t}$, current tidal radius in arcmin.
Column 5: $c \equiv \log_{10}(r_{\rm t}/r_{\rm c})$, concentration.
Column 6: e, ellipticity (projected axial ratio).
Column 7: $t_{\rm rh}$, half-mass relaxation time in years.
Column 8: cluster age in years (taken from the literature, as remarked).

Note that the listed values of c and $r_{\rm c}$ of M15 should not be used to calculate a value of tidal radius $r_{\rm t}$ for this core-collapsed cluster as explained in the catalogue.

A first approximation is achieved by using the age of the system in units of current half-mass relaxation time $(t/t_{\rm rh})$ and the cluster ellipticity. Fig. 5 shows the dependence of ellipticity on the cluster age, where the position of the identified models for six clusters of Table 1 is included. For the model identification, the errors in the cluster age determination (taken from the literature, Table 1) define

Table 1. Globular cluster observational data (see the text for description).

	$r_{\rm c}$ (arcmin)	$r_{\rm h}$ (arcmin)	$r_{\rm t}$ (arcmin)	c	e	$t_{\rm rh}$ (yr)	age (yr)
NGC 104 (47Tuc)	0.40	2.79	42.86	2.03	0.09	3.01×10^9	$1.2 \pm 0.1 \times 10^{10}$ (4)
NGC 2808	0.26	0.76	15.55	1.77	0.12	1.3×10^9	$1.6 \pm 2 \times 10^{10}$ (1)
NGC 5139 (ωCen)	2.58	4.80	44.83	1.24	0.12	1.0×10^{10}	$1.6 \pm 0.3 \times 10^{10}$ (7)
NGC 5286	0.29	0.69	8.36	1.46	0.12	1×10^9	$1.6 \pm 0.2 \times 10^{10}$ (5)
NGC 5904 (M5)	0.42	2.11	28.4	1.83	0.14	3.38×10^9	$13.5 \pm 1 \times 10^9$ (6)
NGC 6093 (M80)	0.15	0.65	13.28	1.95	0.0	7.2×10^8	1.4×10^{10} (2)
NGC 6121 (M4)	0.83	3.65	32.49	1.59	0.0	6.6×10^8	$13.5 \pm 1 \times 10^9$ (6)
NGC7078 (M15)	0.07	1.06	21.50	2.5	0.05	2.23×10^9	$13 \pm 3 \times 10^9$ (3)

References. (1) Alcaino et al. (1990); (2) Brocato et al. (1998); (3) Caputo, Costellani & Cuarta (1984); (4) Grundahl, Stetson & Andersen (2002); (5) Samus et al. (1995); (6) Sandquist et al. (1996); (7) kinematical data from Trager, King & Djorgovski (1995), age from Thompson et al. (2001).
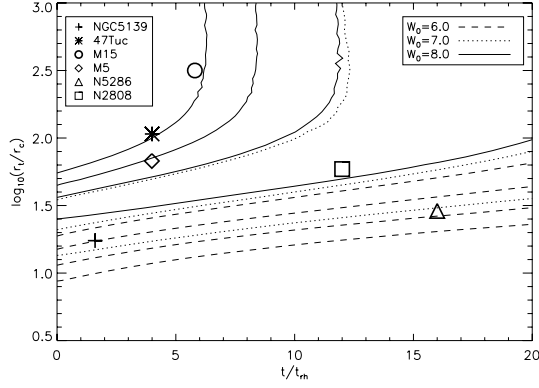
Figure 6. Evolution of concentration. The rotation parameter $\omega_0 = 0.0, 0.3, 0.5, 0.7$ (for $W_0 = 6$), $\omega_0 = 0.0, 0.3, 0.5$ (for $W_0 = 7$) and $\omega_0 = 0.1, 0.15, 0.2, 0.3$ (for $W_0 = 8$) increases from top to bottom at the concentration axis.

age intervals, which match with the computed ellipticity curves. As commented in previous papers (Paper I; Paper II), the observed decrease in ellipticity is not only due to angular momentum loss (evaporation) but also due to the expansion of mass shells retaining their angular momentum and decreasing their angular velocity (inversely to the actual radius of the shell). A coincidence in the behaviour of ellipticity and rotational velocity profiles gives an evidence of rotation in globular clusters (Meylan & Mayor 1986).

As far as concentration and ellipticity are independently computed, we use the age and concentration $c = \log(r_t/r_c)$ of the cluster, in order to make the determination of the model more accurate. Fig. 6 shows the concentration against dynamical age for the same models. Using Figs 5 and 6, one can determine the initial parameters (W_0, ω_0) of the model to use.

Table 2 shows the cluster parameters for GCs of Table 1 with $e > 0$, used to determine the initial conditions of the simulation (W_0, ω_0). First column shows the name of the cluster, second column the observed ellipticity, third column the current concentration, fourth column the age of the cluster in units of half-mass relaxation time and Columns 5 and 6 the initial parameters W_0 (King parameter) and ω_0 (initial rotation).

For the model determination, the coincidence on both, ellipticity and concentration, to observations in Figs. 5 and 6 was located. As these figures could be filled using all possible pairs (W_0, ω_0), we show representative initial parameters and rule out the ones which do not match both initial conditions (e.g. higher ω_0, or lower W_0). Thus, determined models are not unique but representative. Nevertheless, as the models are still idealized, implementation of more complexity in cluster structure (different mass species, stellar evolution) and in interaction with the parent galaxy (tidal shocks, dynamical friction) could affect the results.
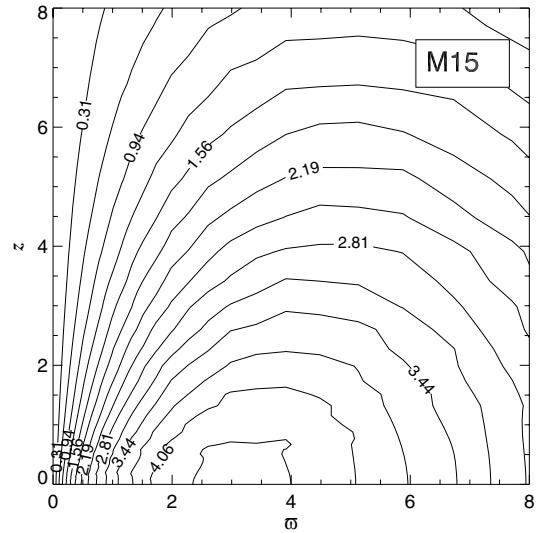
In Figs 7–9 and 11, we present contour plots of the rotational velocity $v_{rot} = \varpi \, \Omega$ in the meridional plane (ϖ, z) for four models

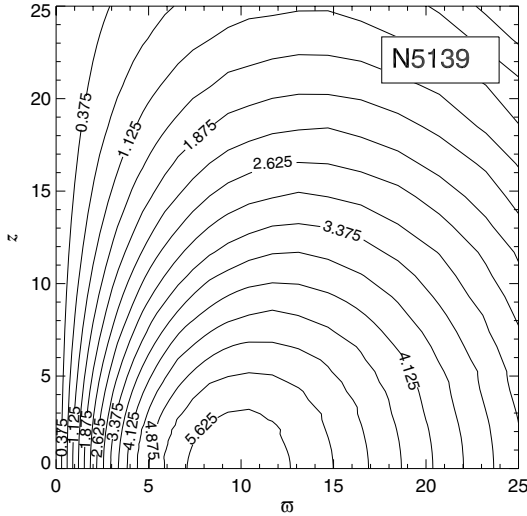**Table 2.** Globular cluster initial models (see the text for description).

	e	c	t/t_{rh}	W_0 (initial)	ω_0 (initial)
47Tuc	0.09	2.03	4.0 ± 0.3	8	0.15
N2808	0.12	1.77	12 ± 1.5	8	0.3
ωCen	0.17	1.24	1.6 ± 0.3	6	0.5
N5286	0.12	1.46	16 ± 0.2	7	0.5
M5	0.14	1.83	3.99 ± 0.3	8	0.2
M15	0.05	2.5	5.8 ± 1.3	8	0.1
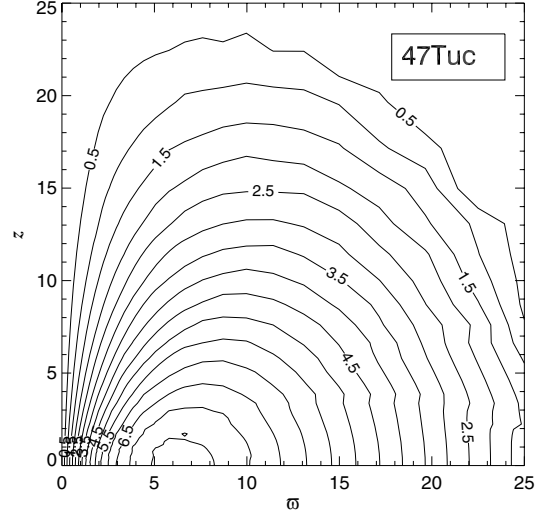
Figure 7. Contour map of rotational velocity for a 47Tuc model. $W_0 = 8$, $\omega_0 = 0.15$ and $t/t_{rh} = 4.0$. Distances are in arcmin and contours are labelled in km s^{-1}.

Figure 8. Same as Fig. 7 for a model of M15. $W_0 = 8.0$, $\omega_0 = 0.1$ and $t/t_{rh} = 5.8$.

of Table 2. v_{rot} was transformed to physical units (km s^{-1}) using an estimation of the total cluster mass according to a mean mass-to-light ratio of M/L = 2 (Harris 1996, 2003 February revision) and using r_c as a length scale. The distances (ϖ and z) are rescaled to arcmin. Single mass pre-collapsed models were used.

Fig. 7 shows a contour map of rotational velocity for an initial model ($W_0 = 8.0, \omega_0 = 0.15$) at $t/t_{rh} = 4$, identified as a 47Tuc model. The maxima of $v_{rot} \sim 7.6$ km s^{-1} is located at ~ 7.7 arcmin. Rotation *HST* measurements of 47Tuc have recently confirmed earlier studies of this globular cluster (Meylan & Mayor 1986; Anderson & King 2003). Anderson & King (2003) found a rotational velocity of 5.7 km s^{-1} at a radius of 7.5 pc. This is quite comparable to the maximum line-of-sight rotation of ~ 6 km s^{-1} at 5 pc (~ 11–$12\, r_c$) found by Meylan & Mayor (1986).

Gerssen et al. (2002) reported the kinematical study of the central part of the globular cluster M15, including v_{rot}. M15 is known as

Figure 9. Same as Fig. 7 for a model of ωCen. $W_0 = 6$, $\omega_0 = 0.5$ and $t/t_{\rm rh} = 1.6$.

Figure 10. Contour plot of the mean azimuthal velocity in the meridional plane of ωCen. Distances are in arcmin and contours are labelled in km s^{-1} (Merritt et al. 1997).

Figure 11. Same as Fig. 7 for a model of M5. $W_0 = 8$, $\omega_0 = 0.2$ and $t/t_{\rm rh} = 4.0$.

a globular cluster which contains a collapsed core. Gebhardt et al. (1994) showed that M15 has a net projected rotation amplitude of $v_{\rm rot} = 2$ km s^{-1} at radii comparable to the half-light radius (about 1 arcmin). Gebhardt et al. (2000) has revealed that the rotation amplitude is larger ($v_{\rm rot} = 10.4 \pm 2.7$ km s^{-1}) at $r \leqslant 3.4$ arcsec, implying that $v_{\rm rot}/\sigma \sim 1$ in this region. Fig. 8 shows the rotational velocity distribution in the meridional plane of a M15 model ($W_0 = 8.0$, $\omega_0 = 0.1$) at $t/t_{\rm rh} = 5.8$. Although our single-mass (and multimass) models can not explain the rapidly rotating central region, this phenomena was already observed in our current simulations of rotating collapsed BH models, which will be topic of a future publication. Note that the core radius of this cluster (0.07 arcmin) requires a better resolution to be able to confirm observational data (see below).

Gerssen et al. (2002, 2003), used *HST* to obtain new spectra of stars in the central cluster region of M15. They found theoretically, that the existence of an intermediate-mass black hole of mass (1.7 ± 2.7) $\times 10^3 M$ can explain the observed velocity dispersion. However, Baumgardt et al. (2003) have shown that the core-collapse profile of a star cluster with an unseen concentration of neutron stars and heavy mass white dwarfs can explain the observed central rise of the mass-to-light ratio. Though, they did not reject the possibility of the presence of IMBHs.

Fig. 9 shows the contour map of rotational velocity for an initial model ($W_0 = 6.0, \omega_0 = 0.5$) at $t/t_{\rm rh} = 1.6$ identified as a ωCen model. The maxima of $v_{\rm rot}$ (6 km s^{-1}) is found at ~ 9 arcmin $\sim 3r_c$. For comparison, Fig. 10 shows the observed two-dimensional rotational structure of ωCen in the meridional plane (Merritt et al. 1997). Using a non-parametric technique on 469 radial velocity data, they obtained a two-dimensional structure of rotational velocity in ωCen and found a peak rotational velocity of 7.9 km s^{-1} at ~ 11 pc, corresponding to ~ 3 times the core radius (r_c). Van Leeuwen et al. (2000) found agreements of proper motion studies with the rotation in this cluster.

Fig. 11 shows the rotation in the meridional plane of a M5 model with a maximum of $v_{\rm rot} = 5.6$ km s^{-1} at about 5 arcmin $\sim 12r_c$. It has one of the highest ellipticities in the Harris catalogue ($e = 0.14$) and the highest in our sample. Currently, there are not observational data of rotation of this globular cluster to compare with.

The simulated profile of $v_{\rm rot}/\sigma$ (rotational velocity over one dimensional velocity dispersion) of four clusters of Table 2 is plotted
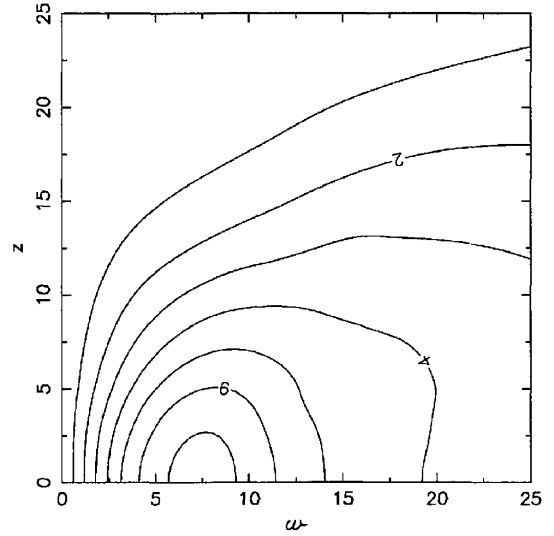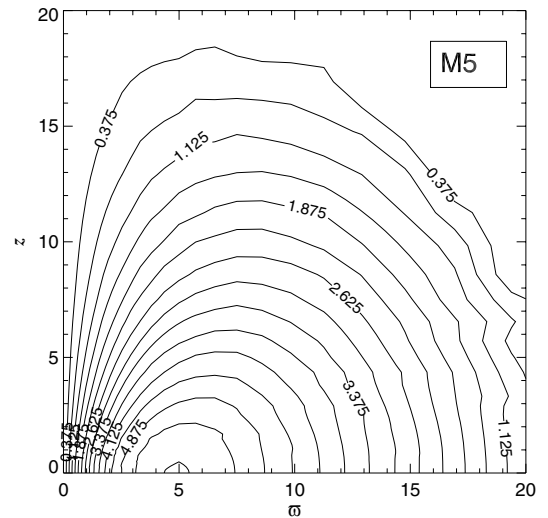
in Fig. 12. They show a maximum of rotation at around the half-mass radius and a rapid decline afterwards, as well as a rigid body rotation in the centre. Note that the maxima of the M15 model is located closer to the centre than the other clusters, as M15 has the largest dynamical age (see Table 2) and dynamical effects as gravogyro instabilities dominate the evolution (Hachisu 1979, 1982). The results show that our data are consistent with observations, as the newly presented in Van de Ven et al. (2006), who show the importance of rotation ($v_{\rm rot}/\sigma$ distribution in the meridional plane) in ωCen at radii of about 5–15 arcmin, however, dropping more inwards and further outwards. Nevertheless, more physical constraints (multimass modes and stellar evolution) are needed in our simulations in order to follow properly the interaction of rotation and relaxation. In the same way, we can obtain data of any model described in Section 4 and in the Appendix.
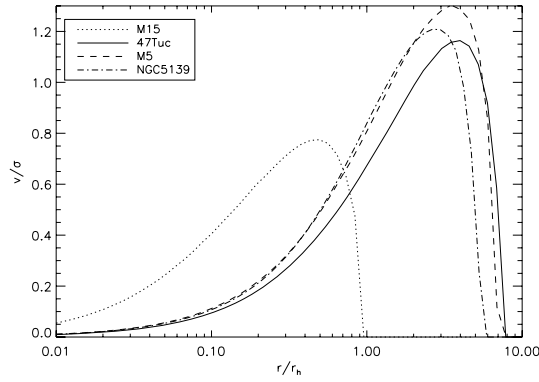
Figure 12. Simulated v/σ plotted against cluster radius, given in units of current half-mass radius.

6 CONCLUSIONS AND OUTLOOK

Most globular clusters are flattened by rotation, and show interesting features in their rotation curves. While rotation is not dominant it is also not negligible, the total amount of rotational (ordered) kinetic energy (as compared to unordered kinetic energy) can be as high as a few 10 per cent typically. Young globular clusters are usually more flattened than older ones. This was observed in the Magellanic clouds (Kontizas et al. 1990; Hill & Zaritsky 2006) and in M31 (Barmby 2002); and theoretically studied (Frenk & Fall 1982; Goodwin 1997; Bekki et al. 2004). However, see also Mackey & van den Berg (2005) for the MW. While observations, especially using the utmost accuracy for single star measurements in globular clusters with the *HST* (e.g. Anderson & King 2003; Rich et al. 2005) provide a marvellous detail of morphological and sometimes surprising kinematical information, people seem sometimes still surprised that even the most elementary feature of flattening and rotation (and its dynamical implication for rotational and dispersion velocities) are so difficult to model and will not be fitted well by multimass King models (Longaretti & Lagoute 1997; Kim et al. 2004). We have provided detailed evolutionary models here which make it possible to compare them easily with observations, using data first obtained by Einsel & Spurzem (1999, Paper I) for the equal mass pre-collapse phase. The basic idea of our data collection, which we have discussed here in a few examples, and which is complete at the web URL http://www.ari.uni-heidelberg.de/clusterdata is that one can go in it using simple global observational data (dynamical age, flattening and/or concentration of a cluster), and then pick from a small number of theoretical evolved models to compare with.

Two-dimensional axisymmetric FP models were used in order to follow the dynamical evolution of rotating stellar systems by using initial parameters (King dimensionless central potential parameter W_0, dimensionless measure of rotational energy ω_0). Our data sample is the only one available from theoretical evolutionary modelling of rotating globular clusters and is aimed to allow direct comparison with observational data, as that presented by Merritt et al. (1997) and Gebhardt et al. (2000), by using our formatted data files and IDL plotting routines provided. Rotation conduces the system to a phase of strong contraction (during a mass and angular momentum loss process) and accelerates the collapse time (gravogyro phase; e.g. Hachisu 1979, 1982). The observed rotational structure in the meridional plane and $v_{\rm rot}/\sigma$ curves (despite of the central region of clusters like M15, discussed in Section 5) can be reproduced by our models. Nevertheless, our

models are still idealized and simplified. Physical scalings, such as time-scales, may change if more effects, such of binaries, are included.

The provided data base of models with theoretical cluster data will make it possible for observers to select model data to compare with.[3] Our data base will in the future be extended to more realism including a stellar mass spectrum and stellar evolution of singles and binaries, which all is subject of ongoing work (Ardi et al. 2005). Also a study of rotating clusters with a central massive star-accreting black hole is under way (Fiestas & Spurzem, in preparation), which will provide important data for galactic nuclei and to check claims that some globular clusters contain intermediate-mass black holes.

ACKNOWLEDGMENT

REFERENCES

Aarseth S. J., 1999a, PASP, 111, 1333
Aarseth S. J., 1999b, Celest. Mech. Dyn. Astron., 73, 127
Aarseth S. J., 2003, Ap&SS, 285, 367
Alcaino G., Liller W., Alvarado F., Wenderoth E., 1990, ApJS, 72, 693
Anderson J., King I. R., 2003, AJ, 126, 772
Ardi E., Spurzem R., Mineshige S., 2005, J. Korean Astron. Soc., 38, 207
Barmby P., Holland S., Huchra J. P., 2002, MNRAS, 123, 1937
Baumgardt H., 2001, MNRAS, 325, 1323
Baumgardt H., Makino J., 2003, MNRAS, 340, 227
Baumgardt H., Hut P., Heggie, D. C., 2002, MNRAS, 336, 1069
Baumgardt H., Hut P., Makino J., McMillan S., Portegies Zwart S., 2003, ApJ, 582, 21
Beccari G., Ferraro F. R., Possenti A., Valenti E., Origlia L., Rood R. J., 2006, AJ, 131, 2551
Bekki K., Beasley M. A., Forbes D. A., Couch W. I., 2004, ApJ, 602, 730
Boily C. M., Spurzem R., 2000, in Noels A., Magain P., Caro D., Jehin E., Parmentier G., Thoul A. A., eds, Proc. 35th Liege Int. Astrophysics Colloquium, The Galactic Halo; From Globular Cluster to Field Stars. Institut d'Astrophysique et de Geophysique, Liege, p. 607
Brocato E., Castellani V., Scotti G. A., Saviane I., Piotto G., Ferraro F. R., 1998, A&A, 335, 929
Caputo F., Castellani V., Cuarta M. L., 1984, A&A, 138, 457
Cohn H., 1979, ApJ, 234, 1036
Drukier G. A., Cohn H. N., Lugger P. M., Yong H., 1999, ApJ, 518, 233
Einsel C., 1996, PhD thesis, Univ. Kiel
Einsel C., Spurzem R., 1999, MNRAS, 302, 81 (Paper I)
Freitag M., Benz W., 2002, A&A, 394, 345
Frenk C. S., Fall S. M., 1982, MNRAS, 199, 565
Gebhardt K., Pryor C., Wiliams T. B., Hesser J. E., 1994, AJ, 107, 2067
Gebhardt K., Pryor C., O'Connell R. D., Williams T. B., Hesser J. E., 2000, ApJ, 119, 1268
Gerssen J., Van der Marel R., Gebhardt K., Guhathakurta P., Peterson R., Pryor C., 2002, AJ, 124, 3270
Gerssen J., Van der Marel R., Gebhardt K., Guhathakurta P., Peterson R., Pryor C., 2003, AJ, 125, 376
Geyer E. H., Nelles B., Hopp U., 1983, A&A, 125, 359
Giersz M., Heggie D. C., 1994, MNRAS, 270, 298
Giersz M., Heggie D. C., 1996, MNRAS, 279, 1037
Giersz M., Spurzem R., 1994, MNRAS, 269, 241
Goodman J., 1983, PhD thesis, Princeton Univ.
Goodwin S., 1997, MNRAS, 286, 39

[3] Look for http://www.ari.uni-heidelberg.de/clusterdata/

Grundahl F., Stetson P. B., Andersen H. I., 2002, A&A, 395, 481

Hachisu I., 1979, PASJ, 31, 523

Hachisu I., 1982, PASJ, 34, 313

Harris W. E., 1996, AJ, 112, 1487 (http://physics.mcmaster.ca/Globular. html)

Heggie D. C., 1984, MNRAS, 206, 179

Hemsendorf M., Dorband N., Merritt D., 2003, in Makino J., Hut P., eds, Proc. IAU Symp. 208, Astrophysical Supercomputing Using Particle Simulations. Astron. Soc. Pac., San Francisco, p. 405

Henyey L. G., Wilets L., Böhm K. H., Levelier R., Levee R. D., 1959, ApJ, 129, 628

Hill A., Zaritsky D., 2006, AJ, 131, 414

Hut P., 1985, in Goodman J., Hut P., eds, Proc. IAU Symp. 113, Dynamics of Star Clusters. Reidel, Dordrecht, p. 231

Kim E., Einsel C., Lee H. M., Spurzem R., Lee H. G., 2002, MNRAS, 334, 310 (Paper II)

Kim E., Lee H. M., Spurzem R., 2004, MNRAS, 351, 220 (Paper III)

Kontizas E., Kontizas M., Sedmak G., Smareglia R., Daperlogas A., 1990, AJ, 100, 425

Kustaanheimo P., Stiefel E., 1965, Reine Angew. Math., 218, 204

Longaretti P. Y., Lagoute C., 1997, A&A, 319, 839

Lupton R. H., Gunn J. E., Griffin R. F., 1987, AJ, 93, 1114

Lynden-Bell D., Eggleton P. P., 1980, MNRAS, 191, 483

Mackey A., van den Bergh S., 2005, MNRAS, 360, 631

Makino J., 2005, J. Korean Astron. Soc., 38, 165

Makino J., Taiji M., 1998, Scientific Simulations with Special Purpose Computers. Wiley, Chichester, p. 239

McLaughlin D. E. et al., 2003, in Piotto G., Meylan S. G., Djorgovski S. G., Riello M., eds, ASP Conf. Ser., Vol. 296, New Horizons in Globular Cluster Astronomy. Astron. Soc. Pac., San Francisco, p. 101

McMillan Stephen L. W., Hut P., 1996, ApJ, 467, 348

Merritt D., Meylan G., Mayor M., 1997, AJ, 114, 1074

Meylan G., Mayor M., 1986, A&A, 166, 122

Mikkola S., Aarseth S. J., 1998, New. Astron., 3, 309

Murphy B., Cohn H., Durisen R., 1991, ApJ, 370, 60

Piotto G., Zoccali M., King I. R., Djorgovski S., Sosin C., Rich R. M., Meylan G., 1999, AJ, 118, 1727

Piotto G. et al., 2002, A&A, 391, 945

Portegies Zwart S., Hut P., Makino J., McMillan S. L. W., 1998, A&A, 337, 363

Pulone L., De Marchi G., Covino S., Paresce F., 2003, A&A, 399, 121

Quinlan G., Shapiro S. L., 1990, ApJ, 356, 483

Rich R. F., Corsi C. E., Cacciari C., Federici L., Fusi Pecci F., Djorgovski S. G., Freedman W. L., 2005, AJ, 129, 2670

Rosenbluth M. N., MacDonald W. M., Judd D. L., 1957, Phys. Rev., 107, 1

Samus N., Ipatov A., Smirnov O., Kravtsov V., Alcaino G., Liller W., Alvarado F., 1995, A&AS, 112, 439

Sandquist E. L., Boite M., Stetson P. B., Hesser J. E., 1996, ApJ, 470, 910

Spitzer L., Hart M., 1971, ApJ, 164, 399

Spurzem R., 1996, in Hut P., Makino J., eds, IAU Symp. 174, Dynamical Evolution of Star Clusters – Confrontation of Theory and Observations. Kluwer, Dordrecht, p. 111

Spurzem R., 1999, J. Comput. Appl. Math., 109, 407

Takahashi K., 1995, PASJ, 49, 547

Takahashi K., 1996, PASJ, 48, 691

Takahashi K., 1997, PASJ, 47, 561

Takahashi K., Portegies Zwart S. F., 2000, ApJ, 535, 759

Thompson I. B., Kaluzny J., Pych W., Burley G., Krzeminski W., Paczyński B., Persson S., Preston G. W., 2001, AJ, 121, 3089

Trager S. C., King I. R., Djorgovski S., 1995, AJ, 109, 218

Van de Ven G., van de Bosch R. C. E., Verdme E. K., de Zeeuw P. T., 2006, A&A, 445, 513

Van Leeuwen F., Le Poole R. S., Reijns R. A., Freeman K. C., de Zeeuw P. T., 2000, A&A, 360, 472

White R. E., Shawl S. J., 1987, ApJ, 317, 246

Zhao B., Bailyn Ch. D., 2005, AJ, 129, 1934

APPENDIX A: DATA DESCRIPTION

Grid of models

In http://www.ari.uni-heidelberg.de/clusterdata/, we present exemplarily a grid of runs of our 2D FP models $W_0 = 3, 6, 9$ and $\omega_0 = 0.0$ (no-rotating), 0.3, 0.6, 0.9 (rotating). The data are classified by ellipticity and age of the system. Following a briefly description of the data.

The initial classification of the models is showed in Table 1 (on the web). (W_0, ω_0) are the, respectively, King and rotational initial parameters. Second table shows the grid of data base. Each point of the grid represents an ellipticity and time interval. The numbers in the cells give the total number of available data sets with the corresponding age–ellipticity relation.

By selecting one grid point, one gets the data sets including following information (see Table A1).

(i) Structural parameters:
concentration $c = \log (r_t/r_c)$, (r_c/r_h), escape energy, total mass and energy at any time of evolution.

(ii) Density $n(\varpi, z)$.

(iii) Angular $[\Omega(\varpi, z)]$ and rotational velocity $v_{rot}(\varpi, z) = \Omega(\varpi, z) \cdot \varpi$.

(iv) One-dimensional total velocity dispersion $\sigma_t(\varpi, z)$, azimuthal velocity dispersion $\sigma_\varphi(\varpi, z)$ and velocity dispersion in meridional plane $\sigma_r(\varpi, z)$.

(v) Potential $\phi(\varpi, z)$ and anisotropy $A(\varpi, z)$.

(vi) Normalized (unnormalized) energy $X(E)$ and angular momentum $Y(J_z)$, and evaluated distribution function $f(E, J_z)$.

Further definitions are as follows.

(i) Escape energy $x_0 \equiv \frac{\phi(r_t) - \phi_c}{\sigma_c^2}$ (ϕ_c is the central potential).

(ii) Core radius r_c (equation 9)

(iii) One-dimensional square velocity dispersion: $\sigma_t(\varpi, z)^2 = \sigma_\phi(\varpi, z)^2 + 2\sigma_r(\varpi, z)^2$, (due to $\sigma_r = \sigma_z$).

(iv) Anisotropy $= 1 - \frac{\sigma_\phi(\varpi, z)^2}{\sigma_r(\varpi, z)^2}$.

(v) Normalized energy $X(E) \equiv \ln \frac{2\phi_c - E - E_0}{E}$.

(vi) Normalized angular momentum $Y(J_z, E) \equiv \frac{J_z}{J_z^{\max}(E)}$.

Evolution in time

Here, we present filtered data classified by initial model parameters (W_0, ω_0) (Table 3 on the web). They include the time evolution of following parameters.

(i) Time in units of half-mass relaxation time (t/t_{rh_i}).

(ii) Time-step number.

(iii) Time in units of central relaxation time (t/t_c).

(iv) Core radius r_c (units of initial core radius $= 1$).

(v) Central density n_c.

(vi) Central rotational velocity v_c.

(vii) Central one-dimensional velocity dispersion σ_c.

(viii) Ellipticity e_{dyn} (equation 10).

(ix) Escape energy.

(x) Collapse rate $\xi \equiv \frac{\tau_{rc}}{n} \frac{dn}{dt}$.

(xi) Total mass (units of initial).

(xii) Total angular momentum (z-component).

(xiii) Total potential energy.

(xiv) Total kinetic energy.

Plots as those presented in this paper are also shown including IDL routines used to generate them.

Table A1. Set of files provided by the data base.

File name	Brief description
GP_[$W_0 \times 10$]_[$\omega_0 \times 100$]_[time step]	Global parameters
RHO_[$W_0 \times 10$]_[$\omega_0 \times 100$]_[time step]	Density
ROTV_[$W_0 \times 10$]_[$\omega_0 \times 100$]_[time step]	Rotational and angular velocity
VDISP_[$W_0 \times 10$]_[$\omega_0 \times 100$]_[time step]	1D velocity dispersion and components
PHI_AN_[$W_0 \times 10$]_[$\omega_0 \times 100$]_[time step]	Potential and anisotropy
DF_[$W_0 \times 10$]_[$\omega_0 \times 100$]_[time step]	Distribution function

This paper has been typeset from a TEX/LATEX file prepared by the author.